J Nondestruct Eval (2016) 35:48
DOI 10.1007/s10921-016-0364-6

Noncontact Sonic NDE and Defect Imaging Via Local Defect Resonance

Igor Solodov[1] · **Markus Rahammer**[1] · **Nikolai Gulnizkij**[1] · **Marc Kreutzbruck**[1]

Received: 17 March 2016 / Accepted: 9 August 2016 / Published online: 16 August 2016

Abstract A selective acoustic activation of defects based on the concept of local defect resonance enables to enhance considerably the intensity of defect vibrations and makes it possible to reduce the input acoustic powers to the levels permissible for noncontact nondestructive inspection. Since for cm-size defects in composite materials, the LDR frequencies lie in the low kHz-range, the resonant noncontact activation shifts to an audible frequency range and can be provided by conventional sonic equipment. In this paper, the feasibility of the resonant noncontact inspection is validated for the most "problematic" methodologies of nonlinear, thermosonic and shearosonic NDE that usually require an elevated acoustic power and, therefore, a reliable contact between the specimen and the transducer. In contrast, the noncontact versions developed employ commercial loudspeakers which can simultaneously insonify large areas and be applied for a contactless sonic inspection of different materials and various scale components.

Keywords Local defect resonance · Shearosonics · Thermosonics

1 Introduction

The interaction of elastic waves with defects is the background of ultrasonic testing and NDE of materials and industrial components. In conventional ultrasonic NDE, this interaction is responsible for sound attenuation and scattering (primary ultrasonic effects) which results in variation of the wave amplitude and phase as indicators of the presence of defects. The derivative ultrasound-induced effects (nonlinear, thermal, acousto-optic) are more advantageous in many cases and also widely used for NDE and defect imaging. However, these effects are usually comparatively inefficient so that the corresponding NDE techniques (nonlinear ultrasonics, ultrasonic shearography (shearosonics) and ultrasonic thermography (thermosonics)) require an elevated acoustic power and differ from conventional NDE set-ups for their specific instrumentation.

An increase in sensitivity of these techniques was found by choosing the wave frequency equal to one of the resonance frequencies of the specimen providing that the defect is outside the nodal areas of the standing wave pattern [1–3]. This condition was found to enhance the nonlinear defect response and was applied in multiple experiments on nonlinear acoustic characterization of materials (e.g. [1,2]). In order to eliminate the effect of nodal lines and to exclude "missing" the defect, the multi-modal frequency excitation was suggested to provide the standing wave pattern, which "hits" the defect [4].

A drawback of single-frequency ultrasonic excitation concerned with the nodal lines was also realized in thermosonics. To increase the probability of detection it was proposed to excite the specimens at multiple resonance frequencies [5]. The frequency selection was aimed at avoiding the areas of low-sensitivity due to nodal line patterns [5] or to providing a particular displacement pattern of a vibrating crack [6]. An enhancement in crack detectability by producing a wide-band excitation ("acoustic chaos") was reported in [7].

Alternative approaches to optimize acoustic response, which are being used in nonlinear acoustics of gas bubbles in liquids [8] introduce a resonance frequency of the bubble as a key factor to increase an ultrasonic response of the insonified inclusion. The discovery of anomalous nonlinear

✉ Igor Solodov
igor.solodov@ikt.uni-stuttgart.de

[1] Institut für Kunststofftechnik (IKT), University of Stuttgart, 70569 Stuttgart, Germany

ultrasonic response of medical contrast agents, whose local nonlinearity enhanced remarkably due to resonance vibrations of incorporated gel bubbles initiated a breakthrough in ultrasonic medical diagnostics [9].

Likewise, in our studies, it was proposed to enhance acoustic response of a defect by using selective acoustic activation of defects based on the concept of Local Defect Resonance (LDR) [10]. In the general case, the presence of a defect apparently leads to a local decrease in stiffness for a certain mass of the material around the damaged area, which should manifest in a particular characteristic frequency (f_0) of the defect. The frequency match between the driving wave (frequency f) and f_0 results in the high-amplitude defect resonance vibrations and thus provides an efficient delivery of acoustic energy directly into the defect. The resonance acoustic response ensures a boost in efficiency and sensitivity of defect detection and imaging by using both primary and secondary ultrasonic effects.

The enhanced input-output conversion efficiency also enables to decrease an input acoustic power down to μW-mW [11] and opens an opportunity for remote activation of defects by using air-coupled ultrasonics (ACU) [12]. However, according to our measurements, for cm-size defects in composite materials, the LDR frequencies lie in the low kHz-range. It enables a drastic modification of resonant NDE by providing noncontact activation in the sonic frequency range. The sound sources can simultaneously insonify large areas and be applied for remote resonant sonic NDE of different materials and various scale components.

In this paper, we present the methodology and the case studies of sonic imaging of defects by using noncontact versions of nonlinear laser vibrometry, thermosonic and shearosonic NDE techniques.

2 Airborne Sonic Activation of Defects

The three types of apparatuses used for sonic activation of defects were as follows:

- Commercial dynamic loudspeakers JBL Control One with RMS power of 150 W. The LF-section of the loudspeakers provides excitation in the frequency range 2–6 kHz, while the HF-speakers—from 8 to 19 kHz. The input signal to the speakers comes from the Integrated Stereo amplifier NAD 319 (20 Hz–20 kHz frequency response; 280 W max continuous power). For input voltages 3–35 V, the sound intensity varied in the range of 85–100 dB.
- A Long Range Acoustic Device (LRAD) which provided sound intensity of 132 dB within 30° beam in a continuous output mode. The LRAD frequency response is limited to the range from 2.5 to 9 kHz with maximum output between 3 and 5 kHz.

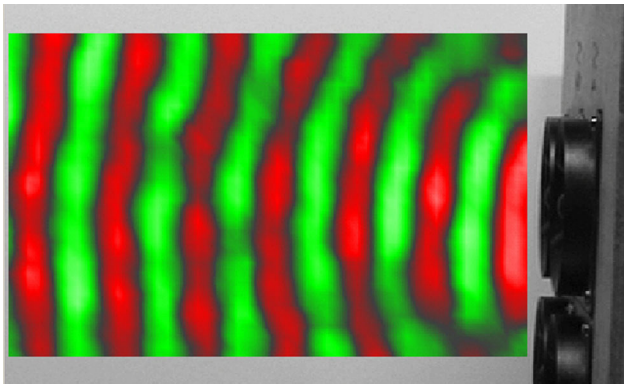

Fig. 1 Air-coupled vibrometry of 10 kHz sound field radiated by a piezoelectric loudspeaker

- Piezoelectric loudspeakers CTS 232 with max frequency response between 4 and 14 kHz. The maximum sound intensity achievable was measured within 120–130 dB range.

To quantify the sound field produced we used the air-coupled vibrometry technique [13], which relates the laser vibrometer readings of "virtual" Doppler velocity V and the amplitude of vibration velocity $\Delta V_{\sim}$ in the sound field:

$$\Delta V_{\sim} \approx 3.5 \times 10^3 (KL)^{-1} V, \tag{1}$$

where K is the sound wave number and L is the sound field aperture.

An example of the visualized sound field radiated by a piezo-speaker and used for estimations in (1) is shown in Fig. 1. The vibration velocity was measured directly at the "output" of the sound source (at 1–2 cm distance) where $L \approx$ diameter of the loudspeaker. The sound intensities given above were derived from $\Delta V_{\sim}$ values at this position and reduced apparently with the distance due to spherical divergence. The sound sources were positioned at a distance of 30–150 cm from either front or reverse surface of the specimens. Both normal and slanted incidence set-ups were tested; the latter was particularly useful for avoiding a direct heat flow from the sound source in thermosonic measurements.

2.1 Remote Sonic Nonlinear NDE

Nonlinear acoustic NDE recognised as a promising technology for diagnostics of incipient damage is based on the frequency conversion (e.g. generation of higher harmonics, mixing frequencies) due to a strong nonlinearity of defects caused by Contact Acoustic Nonlinearity (CAN) [14]. The use of LDR, which "amplifies" local defect vibrations, enables to enhance the sensitivity of the technique and realize its noncontact nonlinear version for the first time.

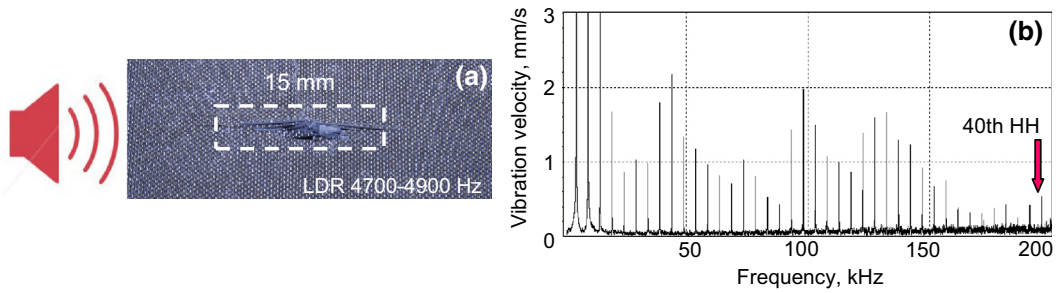

Fig. 2 Impact-induced damage in CFRP specimen used for noncontact nonlinear laser vibrometry (**a**); HH spectrum in the defect area (**b**)

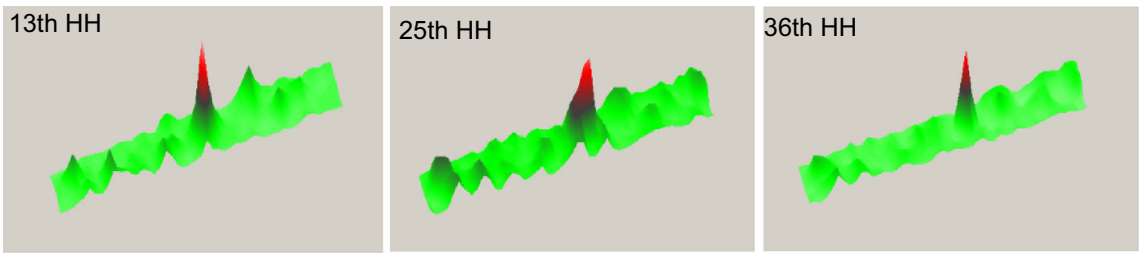

Fig. 3 Noncontact resonant imaging of the defect in Fig. 2 at various higher harmonics. The scanning area is 100 × 20 mm^2

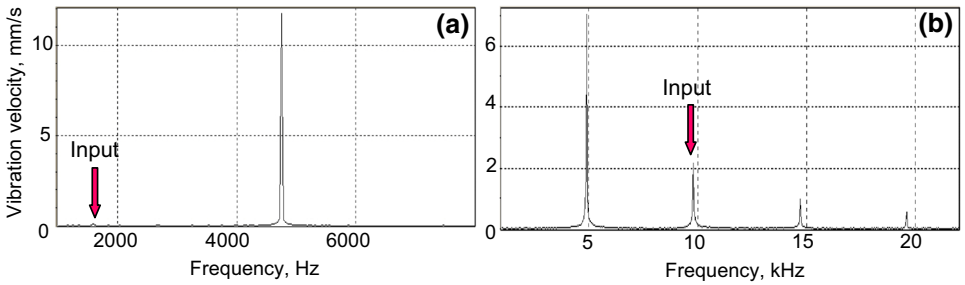

Fig. 4 Third superharmonic (**a**) and subharmonic (**b**) resonances for the impact damage defect in CFRP

The impact damage in CFRP plate (270 × 40 × 1 mm^3, Fig. 2a) was activated by airborne sound at LDR with the frequency response $f_0 = 4700-4900$ Hz (LDR frequency may vary depending on clamping conditions). The dynamic speaker was positioned at a distance of 20–30 cm from the specimen surface; the maximum defect activation was found for a slanted incidence of sound onto the specimen surface at an angle of about 30–45°. The amplitude of the plate wave excited in the CFRP plate measured with a laser vibrometer ranged from 10^{-9} to 5×10^{-8} m. For the wave amplitude 5×10^{-8} m, the LDR "amplification" of 25 dB increased the local vibration amplitude to 0.85 μm sufficient for triggering defect nonlinearity.

The nonlinear vibration spectrum recorded in the defect area (Fig. 2b) demonstrates a strong nonlinearity: more than 40 higher harmonics (HH) are generated due to a strong nonlinearity of the defect. A single area scan of the specimen is then used for mapping the amplitudes of the HH over its surface and therefore results in a number of defect images (Fig. 3). The multitude of the nonlinear images for a single measurement enables to select the images with a high signal-to-noise ratio (SNR). An important feature of the nonlinear images is also concerned with repeatability of the image position, which increases the probability of defect detection.

The combination of CAN and LDR makes a cracked defect a strongly nonlinear oscillator that is known to feature the nonlinear and parametric resonances [15] also applicable for nonlinear NDE and defect imaging [16]. The opportunity for a noncontact excitation of this type of defect vibrations is illustrated in Fig. 4 for the impact damaged CFRP discussed above. When the driving frequency is a fraction of the resonance frequency the defect responds at its LDR frequency (superharmonic resonance). In Fig. 4a, the third-order superharmonic resonance (the peak at $f_0 = 4800$ Hz) develops in the defect area when the input frequency is $f_0/3 = 1600$ Hz. Likewise, the input at double LDR frequency ($f = 2f_0 = 9800$ Hz) results in a sub-harmonic resonance ($f_0 = f/2 = 4900$ Hz) and the integer multiples $nf_0 = nf/2$ of the LDR frequency (Fig. 4b).

The super- and subharmonic resonance frequency components are generated locally within the defect area and,

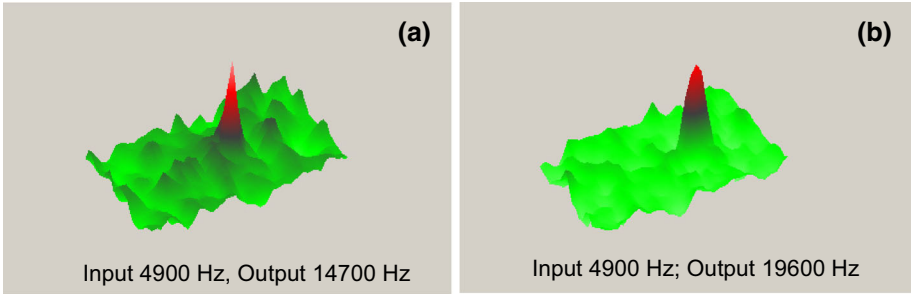

Fig. 5 Noncontact resonant imaging of the impact damage at the third subharmonic (**a**) and the second harmonic/fourth subharmonic (**b**) frequencies. The scanning area is 45×30 mm^2

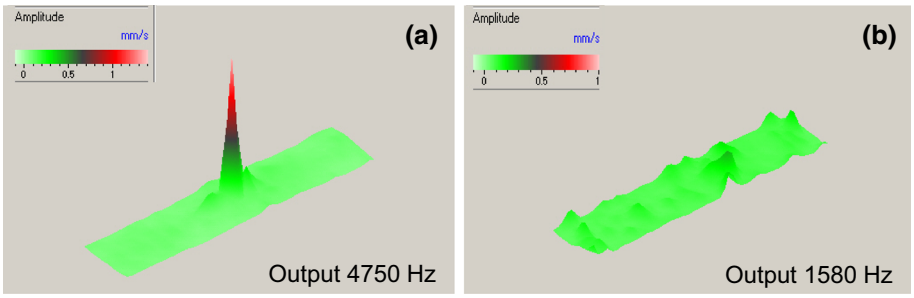

Fig. 6 Noncontact superharmonic (**a**) and non-resonant linear imaging (**b**) of the impact damage for input frequency 1580 Hz

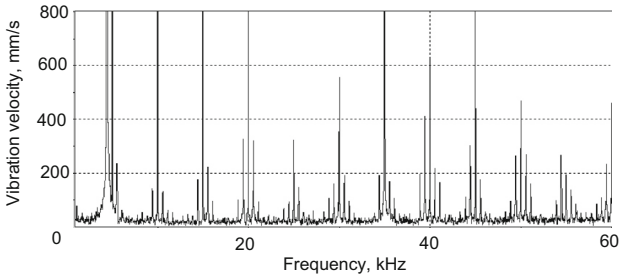

Fig. 7 Frequency mixing spectrum in the impact damage area for input frequencies $f_1 = 4450$ Hz and $f_2 = 5000$ Hz

therefore, are readily applied for imaging of defects. Such an opportunity is demonstrated in Fig. 5a for the third subharmonic ($3f/2 = 14{,}700$ Hz) and compared with combined image at the second harmonic/fourth subharmonic ($2f = 4f/2 = 19{,}600$ Hz) of the driving frequency (Fig. 5b).

An example of the superharmonic imaging is shown in Fig. 6 for the third-order resonance: Input frequency $f = f_0/3 = 1580$ Hz and output is at $f_0 = 4750$ Hz. A good SNR due to LDR is clearly seen for the nonlinear image (a) while the linear image (at the driving frequency) is obviously out of resonance (Fig. 6b).

Another option of nonlinear LDR imaging is concerned with frequency mixing components generated in a dual-frequency excitation. To enhance the efficiency of the nonlinear mixing the excitation frequencies are positioned around the LDR bandwidth to make use of resonant amplification of interacting waves. In the experiment, the impact damage in CFRP was insonified with sound waves radiated by the loudspeakers at frequencies $f_1 = 4450$ and $f_2 = 5000$ Hz. The spectrum of LDR vibrations (Fig. 7) demonstrates that multiple mixed frequency components are generated well described by $mf_1 \pm nf_2$ combination produced by the $(m+n)$-order of nonlinear interaction. Each of the side-lobe frequencies in Fig. 7 is an indicator of the defect presence and position as seen from Fig. 8 where a few examples of the higher-order mixing frequency images are given.

3 Noncontact Resonance Thermosonics

The experimental setup combines a resonant airborne ultrasonic excitation with IR imaging. For noncontact thermosonics, the airborne sound intensity somewhat higher than 100 dB was required so that the piezoelectric speakers and the LRAD were applied for defect imaging given below. The thermal defect response at LDR frequency is measured and visualized with an IR-camera (IRCAM Equus 327K, NETD $\approx$ 15−20 mK). To enhance the sensitivity the lock-in thermosonic mode [17] was used: the input signal to the speakers was amplitude modulated at a low (0.01–0.1 Hz) lock-in frequency. The temperature image sequence of the surface was recorded over a few periods of the lock-in frequency and a discrete Fourier transformation at this frequency is applied to compress this image sequence into a pair of the amplitude and phase images.

Figure 9b shows a thermosonic (phase) image of a circular flat bottomed hole (FBH) in a polymethylmethacrylate (PMMA), also known as acrylic glass) plate (a) obtained with remote excitation by a piezo-speaker at its LDR frequency 8180 Hz. The two period lock-in frequency (0.01 Hz) signal used indicates a small (about 20 mK) but measurable temperature variation inside the FBH induced by the sound

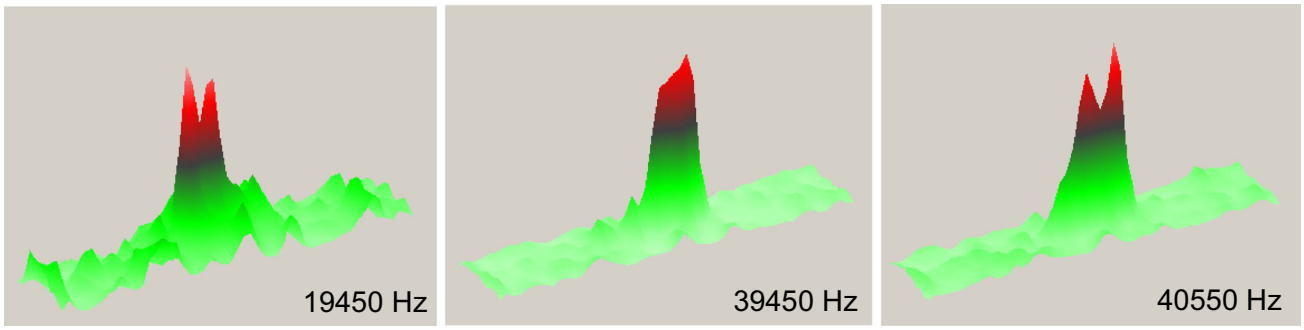

Fig. 8 Remote frequency mixing imaging of the impact damage for the input frequencies $f_1 = 4450$ Hz and $f_2 = 5000$ Hz. The output frequencies are indicated on the *images*

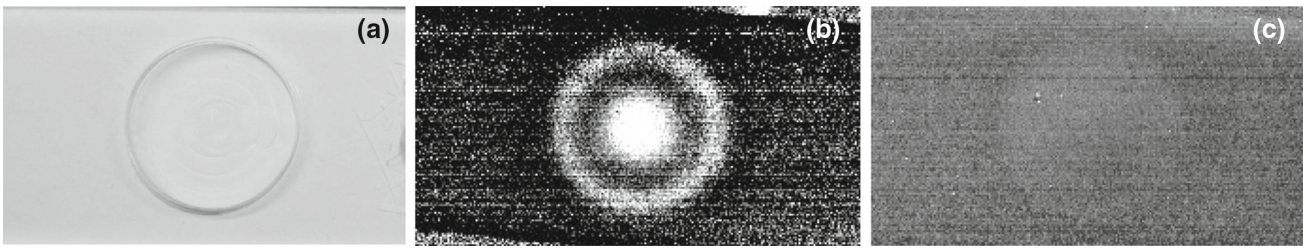

Fig. 9 Remote thermosonic imaging of a circular FBH (**a**) in PMMA plate: phase images at LDR frequency 8180 Hz (**b**) and at 9000 Hz

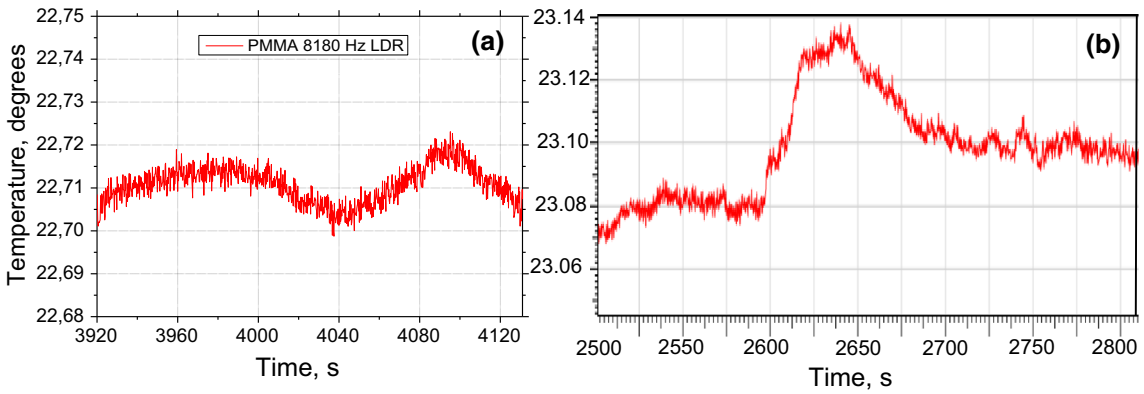

Fig. 10 Temperature variation in remote thermosonic imaging of: **a** FBH in Fig. 9 (2 period of 0.01 Hz lock-in frequency excitation); **b** impact damage in Fig. 11 (1 period of 0.01 Hz lock-in frequency excitation)

modulation (Fig. 10a). As discussed in [11], the shape of the image with an additional concentric circle in Fig. 9 is a characteristic temperature response of a FBH driven in a fundamental LDR mode. It is (along with the temperature plot in Fig. 10a), therefore, an indicator of the lack of spurious heat flow from the sound source and the proof for a sound-driven resonant image, which actually disappears for a minor sound frequency mismatch (Fig. 9c).

Figure 11 illustrates the application of non-contact thermosonics to realistic defects of impact damage in CFRP plate. The LDR frequency of the defect measured with laser vibrometry was found to be around 3600 Hz. The photo of the specimen (Fig. 11a) indicates merely the fiber loss area induced by the impact. The remote thermosonic image at LDR frequency (Fig. 11b) shows that the damaged area is not only localized around the impact but is also extended to the lower edge of the plate. To obtain the remote one-period lock-in frequency phase image in Fig. 11b) the airborne sound intensity was increased up to 130 dB (LRAD) to result in the temperature variation of about 60 mK (Fig. 10b). The shape of the damage in the thermosonic image is readily confirmed by 200 kHz air-coupled ultrasonic C-scanning (the Ultran focused transducers) in Fig. 11c. The benefit of LDR disappears as soon as the driving frequency deviates from the defect resonance frequency (4000 Hz excitation; Fig. 11d).

Another example given in Fig. 12 shows that remote thermosonic imaging is possible for the lower sound intensity. A locally heat damaged CFRP plate ($300 \times 300 \times 4$ mm^3,

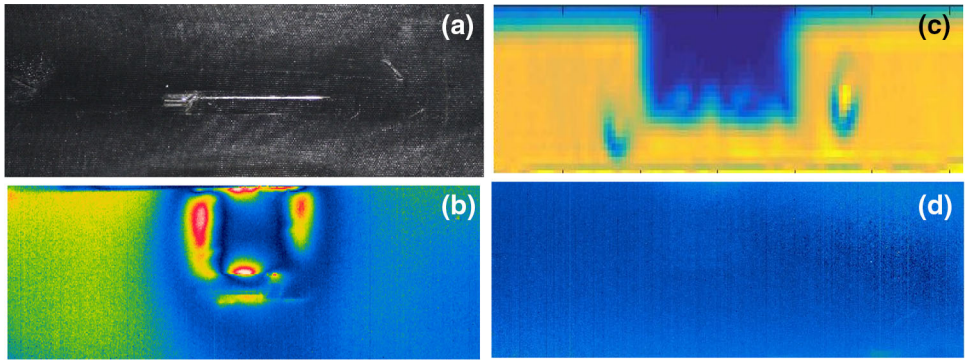

Fig. 11 Noncontact imaging of damage in a CFRP plate (**a**): Remote resonant thermosonic image at LDR frequency 3600 Hz (**b**); ACU image (**c**); thermosonic image at 4000 Hz (**d**)

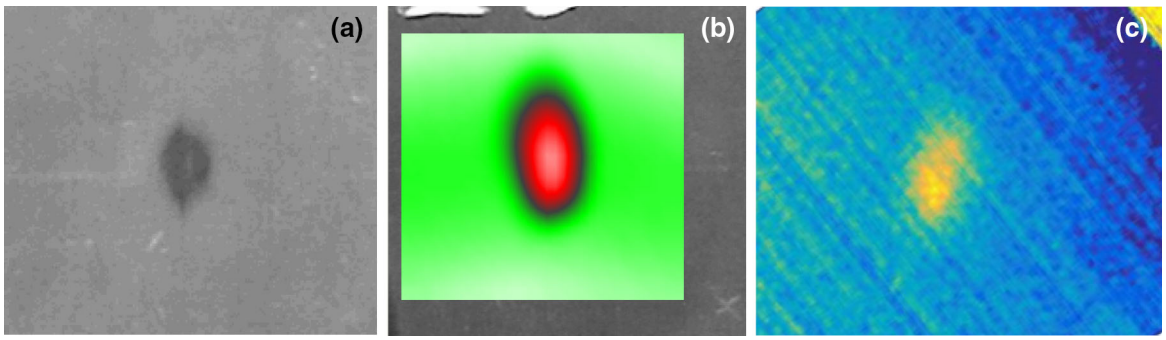

Fig. 12 Noncontact imaging of heat damage ($\sim 10 \times 15$ mm^2) (**a**) in a CFRP specimen: remote laser vibrometry image indicating LDR frequency at 9500 Hz (**b**); thermosonic image at the LDR frequency (**c**)

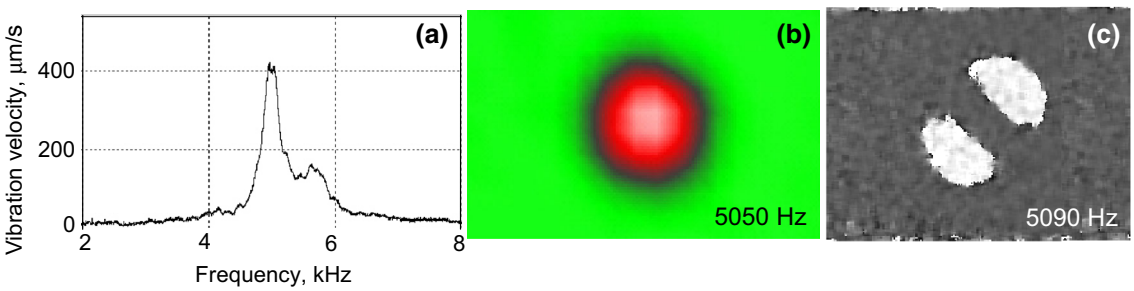

Fig. 13 LDR frequency response (**a**) and noncontact imaging of a circular FBH in a PMMA plate at LDR frequencies: laser vibrometry (**b**) and shearosonic (**c**) images

Fig. 12a) is insonified by airborne sound from the piezoelectric loudspeaker and exhibits LDR at 9500 Hz revealed by laser vibrometry scanning (Fig. 12b). The sound intensity of around 120 dB was measured to be sufficient for noncontact imaging of the defect in a resonant lock-in thermosonic mode shown in Fig. 12c.

4 Remote Shearosonics

In the noncontact shearosonic mode, even moderate sound intensities below 100 dB radiated by dynamic loudspeakers was found to be sufficient for LDR imaging of majority of defects studied. An optical unit used in the experiments comprised a conventional out-of-plane sensor head with continuous-wave laser and CMOS digital camera (frame rate 200 Hz) [18]. The speckle pattern of a vibration object is integrated over the frame period and compared with a reference (undeformed state) speckle. Due to the LDR-induced local resonant increase in defect vibration the sensitivity and the contrast of imaging was expected to enhance substantially.

This fact is illustrated in Figs. 13 and 14 for a circular FBH (radius 1 cm) in PMMA specimen. The frequency response of the defect measured with laser vibrometry for airborne excitation (chirp input) reveals the LDR frequency at around 5000 Hz (Fig. 13a). The laser vibrometry (b) and shearosonics (c) deliver the high-contrast images while excited within LDR frequency band. In accord with the defect resonance response (Fig. 13a), the contrast of the shearosonic imaging decreases dramatically with the frequency mismatch until the

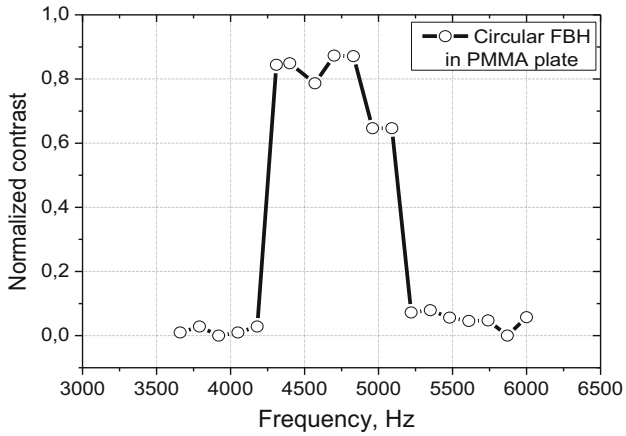

Fig. 14 Normalised contrast for noncontact shearosonic imaging of a circular FBH (see Fig. 13) as a function of driving frequency

image fully disappears in the frequency ranges below 4200 and beyond 5500 Hz excitation (Fig. 14).

A similar resonance contrast enhancement is seen in Fig. 15 for noncontact imaging of a circular disbond (5 cm diameter) in a (100 × 100 × 3 mm^3) CFRP plate. The laser vibrometer and shearosonic images of the disbond obtained at the fundamental LDR frequency (≈3900 Hz) are compared. The "butterfly" fringe pattern (Fig. 15b) clearly demonstrates that shearography is sensitive to the gradient of out-of-plane LDR displacement ("bell-like" function in Fig. 15a) in the shearing direction. The shearosonic imaging of the deformation pattern unlike the vibration velocity field measured with laser vibrometry might be the reason for a slight difference between the LDR frequencies identified with these techniques.

The remote mode was then tested for an artificial delamination (27 × 27 mm^2) (Fig. 16a) at 1.2 mm depth in a large CFRP plate (300 × 300 × 5 mm^3) with LDR frequency around 9000 Hz (b). The loudspeaker was positioned at a distance of about half a meter beside the specimen providing a slanted incidence (∼45°) of sound. To identify the effect of LDR on the defect activation, the frequency of the input signal to the loudspeaker was swept in the range 8–10 kHz and shearosonic images were recorded. The images obtained at LDR frequency (9050 Hz) and outside LDR (10000 Hz) are shown in Fig. 16c, d. The effect of resonant airborne sound activation is clearly seen and results in remote shearographic imaging at LDR frequency of the defect.

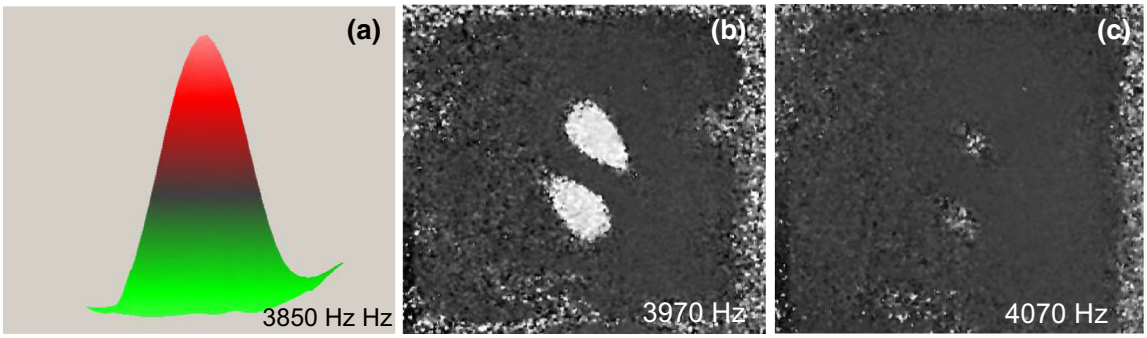

Fig. 15 Noncontact shearosonics of a disbond (LDR frequency 3850 Hz—**a**) in CFRP plate: imaging at LDR frequency (**b**) and outside LDR band (**d**)

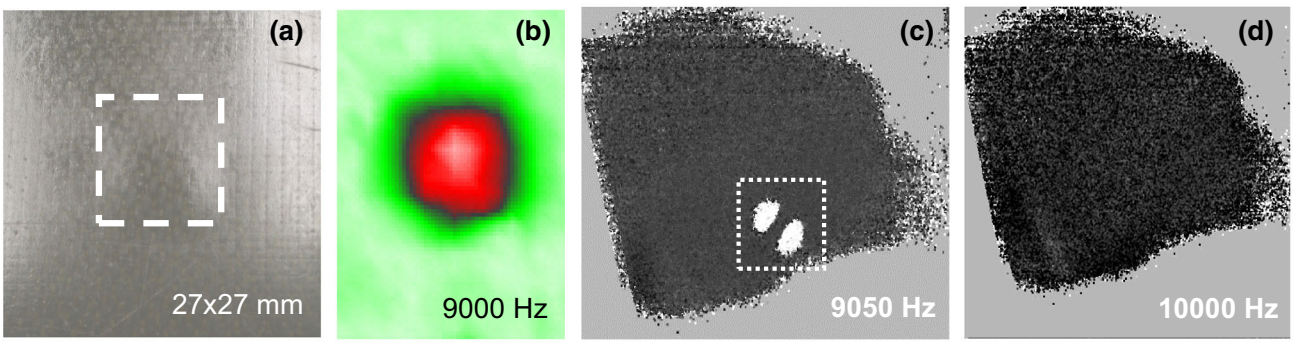

Fig. 16 Noncontact shearosonics of a square insert in CFRP plate (**a**): imaging at LDR frequency (**b** laser vibrometry; **c** shearosonics) and outside LDR band (**d**)

5 Conclusions

The resonant vibrational response of a defect entails a boost in efficiency and sensitivity of defect detection and imaging by using derivative elastic wave effects (nonlinear, thermal, acousto-optic) and opens an opportunity for a noncontact application of these generally low-efficient NDE techniques. For moderate size defects, the resonance occurs in audible frequency range so that NDE inspection can be provided by conventional sonic equipment.

The airborne sound intensities in the range of 100–130 dB radiated by commercial loudspeakers are found to be sufficient for remote detection and imaging of various defects in composite materials via nonlinear, thermosonic and shearosonic NDE techniques. The non-contact versions based on the higher harmonic/frequency mixing as well as super- and subharmonic resonant interactions are feasible and applicable for nonlinear defect imaging. A measurable thermosonic response is observable for remote airborne activation at LDR frequencies for various realistic defects in composites. The resonance sonic shearography provides high contrast noncontact defect imaging even for moderate sound intensities below 100 dB. Conventional loudspeaker systems used can simultaneously insonify rather large areas and applied for remote sonic inspection of different materials and various scale components.

Acknowledgments One of the authors (I.S.) acknowledges support of this study in the framework of ALAMSA project funded from the European Union's Seventh Framework Programme for research, technological development and demonstration under grant agreement no. 314768.

References

1. Guyer, R., Johnson, P.: Nonlinear mesoscopic elasticity: evidence for a new class of materials. Phys. Today **52**, 30–36 (1999)
2. Fillinger, L., Zaitsev, V., Gusev, V., Castagnede, B.: Wave self-modulation in an acoustic resonator due to self-induced transparenc. Europhys. Lett. **76**(2), 229–235 (2006)
3. Renshaw, J., Holland, S., Thompson, R.B.: Measurement of crack opening stresses and crack closure stress profiles from heat generation in vibrating cracks. Appl. Phys. Lett. **93**(8), 081914 (2008)
4. Van Abeele, K.E.-A.: Multi-mode nonlinear resonance spectroscopy for defect imaging: an analytical approach for the one-dimensional case. Acoust. J. Soc. Am. **122**(1), 73–90 (2007)
5. Homma, C., Rothenfusser, M., Baumann, J., Shannon, J.: Study of the heat generation mechanism in acoustic thermography. AIP Conf. Proc. **820**, 566–573 (2006)
6. Rothenfuser, M., Homma, C.: Acoustic thermography: vibrational modes of cracks and the mechanism of heat generation. AIP Conf. Proc. **760**, 624–631 (2005)
7. Han, X., Zheng, Z., Li, W., Islam, M.S., Lu, J., Loggins, V., Yitamben, E., Favro, L.D., Newaz, G., Thomas, R.L.: Acoustic chaos for enhanced detectability of cracks by sonic infrared imaging. J. Appl. Phys. **95**(7), 3792–3797 (2004)
8. Lauterborn, W.: Numerical investigation of nonlinear oscillations of gas bubbles in liquids. J. Acoust. Soc. Am. **59**(2), 283 (1976)
9. Averkiou, M.A.: Tissue harmonic imaging. Proc. IEEE Ultrason. Symp. **2**, 1563–1572 (2000)
10. Solodov, I., Bai, J., Bekgulyan, S., Busse, G.: A local defect resonance to enhance acoustic wave-defect interaction in ultrasonic nondestructive evaluation. Appl. Phys. Lett. **99**(21), 211911 (2011)
11. Solodov, I., Rahammer, M., Derusova, D., Busse, G.: Highly-efficient and noncontact vibro-thermography via local defect resonance. QIRT J. **12**(1), 98–111 (2015). doi:10.1080/17686733.2015.1026018
12. Solodov, I., Busse, G.: Resonance ultrasonic thermography: highly efficient contact and air-coupled remote modes. Appl. Phys. Lett. **102**, 061905 (2013). doi:10.1063/1.4792236
13. Solodov, I., Döring, D., Busse, G.: Air-coupled laser vibrometry: analysis and applications. Appl. Opt. **48**, C33–C37 (2009)
14. Solodov, I., Krohn, N., Busse, G.: CAN: an example of nonclassical acoustic nonlinearity in solids. Ultrasonics **40**, 621–625 (2002)
15. Kneubuehl, F.K.: Oscillations and Waves. Springer, Berlin (1997)
16. Solodov, I.: Resonant acoustic nonlinearity of defects for highly-efficient nonlinear NDE. J. Nondestruct. Eval. **33**, 252–262 (2014)
17. Busse, G., Wu, D., Karpen, W.: Thermal wave imaging with phase sensitive modulated themography. J. Appl. Phys. **71**, 3962–3965 (1992)
18. Menner, Ph, Gerhard, H., Busse, G.: Remote defect visualization with thermal phase angle shearography. AIP Conf. Proc. **1211**(1), 2068–2072 (2010)